Catalysis Communications 89 (2017) 117–120

Contents lists available at ScienceDirect

Catalysis Communications

journal homepage: www.elsevier.com/locate/catcom

Short communication

Oxygen vacancy induced enhancement of photochemical water oxidation on calcium manganese oxide catalyst

Guan Zhang [a,*], Wenyi Dong [a], Xiubing Huang [b], Jing Zou [c]

[a] Shenzhen Key Laboratory of Water Resource Utilization and Environmental Pollution Control, School of Civil and Environmental Engineering, Harbin Institute of Technology, Shenzhen, Shenzhen 518055, PR China
[b] School of Materials Science and Engineering, University of Science and Technology Beijing, Beijing 100083, PR China
[c] School of Humanities & Social Science, The Chinese University of Hong Kong, Shenzhen, Shenzhen 518100, PR China

ARTICLE INFO

Article history:
Received 29 July 2016
Received in revised form 24 October 2016
Accepted 30 October 2016
Available online 01 November 2016

Keywords:
Water oxidation
Calcium manganese oxide
Photo(electro)catalysis
Keywords:
Water oxidation
Calcium manganese oxide
Photo(electro)catalysis

ABSTRACT

The oxygen-deficient $Ca_2Mn_2O_5$ perovskite nanoparticles exhibit remarkably higher catalytic activity compared to $CaMnO_3$ and MnO_2 nanoparticles for photochemical water oxidation. The fraction of surface adsorbed hydroxyl groups on these catalysts has been suggested to be the dominant factors affecting water oxidation activity compared to the other parameters such as oxidation states of manganese and crystal structure.

1. Introduction

The photo(electro)chemical splitting water into hydrogen and oxygen has attracted tremendous attention in recent years because of its great potential in solar energy conversion and storage applications [1]. In respect to hydrogen evolution reaction, a two-electron-transfer process, oxygen evolution reaction is more complex, which involves four-electron-transfer process. Currently, owing to the slow four-electron transfer rate and the high activation energy barrier for O—O bond formation, the oxygen evolution is the main obstacle limiting the efficiency of overall water splitting [2]. Searching environmentally-friendly and efficient oxygen evolution catalysts (OECs) is an urgent and challenging task among the solar water splitting community.

In nature, a Mn_4CaO_5 cluster as the oxygen evolving complex in photosystem II (PS II), has been identified as the catalytic site for the four-electron involved water oxidation [3]. Inspired by the natural photosynthesis process in PS II, synthetic manganese-containing compounds are thought to be very promising candidates as functional water oxidation catalysts to mimic the role of Mn_4CaO_5 cluster in water oxidation [4]. Various nanostructured solid manganese oxides (MnO_x) including MnO_2, Mn_2O_3, Mn_3O_4, MnO_x, MnO, $Mn_3(PO_4)_2 \cdot 3H_2O$, $CaMn_2O_4 \cdot xH_2O$ and amorphous Ca_xMnO_y have been synthesized and tested as OECs in either electrochemical or photochemical systems [5–12].

Recently, oxygen deficient $CaMnO_{3-\delta}$ compounds have been reported as electrocatalysts for oxygen evolution/reduction reactions [13,14]. The results suggest that the oxygen-deficient $CaMnO_{3-\delta}$ compounds are promising and inexpensive bifunctional catalytic materials for reversible oxygen reduction and evolution reactions. Therefore, it is highly desirable to further investigate the oxygen-deficient $CaMnO_{3-\delta}$ as the OECs in a photochemical system for potential application in solar water splitting. In this work, we have synthesized $CaMnO_3$ and $Ca_2Mn_2O_5$ perovskite nanoparticles and evaluated their photocatalytic performance in water oxidation with α-MnO_2 nanorods as a reference sample.

2. Experimental

2.1. Catalysts preparation

The synthesis of $CaMnO_3$ was done by a sol-gel method with citric acid as complexing agent and detailed procedure was shown in

* Corresponding author.
E-mail address: zhangguan@hitsz.edu.cn (G. Zhang).

http://dx.doi.org/10.1016/j.catcom.2016.10.035
1566-7367/

supporting information. The as-prepared $CaMnO_3$ powder was reduced under Ar-5% H_2 at 400 °C for 3.0 h in a tube furnace to get single phase $Ca_2Mn_2O_5$ powder. Nanostructured δ-MnO_2 was prepared according to the literature [15].

2.2. Characterization of catalysts

The reflective XRD pattern was recorded on a PANalytical X-ray diffractometer with graphite-monochromatized Cu K_α radiation (λ = 1.5418 Å), employing a scan rate of $1.5°\cdot min^{-1}$ in the 2θ range of 10° to 100°. The microstructures of samples were inspected by scanning electron microscopy (SEM) on a JEOL 6700F scanning electron microscope. X-ray photoelectron spectroscopy (XPS) was performed using an X-ray photoelectron spectrometer (a monochromated Al KR x-ray source, thermos Escalab 250). The BET surface area of the samples were determined based on the N_2 adsorption isotherms at 77 K with a Coulter Omnisorp 100 CX apparatus.

2.3. Photochemical water oxidation experiments

Photochemical water oxidation experiments were performed in a 0.65 L home-made quartz reactor equipped with a water jacket for cooling. A typical water oxidation experiment was carried out using $[Ru(bpy)_3]Cl_2\cdot 6H_2O$ (100 μM) as a photosensitizer, $Na_2S_2O_8$ (10 mM) as sacrificial electron acceptor in 100 mL borate buffer solution (pH 9) along with the catalyst (25 mg). The reactants were purged with Ar for 1 h to remove all dissolved oxygen from the aqueous solution. The quartz reactor was then illuminated using a 250 W iron-doped halide UV–vis lamp with an ultraviolet cutoff filter (>420 nm). The evolved oxygen gas in the headspace of reactor under irradiation was then examined intermittently using an online gas chromatograph (Agilent 3000 Micro Gas Chromatograph).

3. Results and discussion

3.1. Characterization of catalysts

Pure $CaMnO_3$ was prepared via a sol-gel process and single phase $Ca_2Mn_2O_5$ was obtained through the reductive calcination of as-prepared $CaMnO_3$ under 5% H_2/Ar atmosphere according to the literature [14]. α-MnO_2 nanorods were prepared by thermal treatment of layered δ-MnO_2 at 600 °C for 3 h [15]. Fig. 1 displays the powder XRD patterns and their structures of the different manganese oxide samples. The $CaMnO_3$ sample exhibits typical orthorhombic (*Pnma*) phase structure (JCPDS No. 76-1132), whereas the peaks of $CaMnO_3$ are splitted at around 2θ of 34°, 48° and 60° after reduction, which can be indexed to a different structure (*Pbam*) of $Ca_2Mn_2O_5$ (JCPDS No. 76-1133). In addition, the intensities of $CaMnO_3$ peaks were slightly reduced after reduction due to the crystal distortion and oxygen vacancy formation. The peaks of MnO_2 can be assigned to α-MnO_2 (JCPDS 44-0141) with a tetragonal phase. The intensities and widths of the diffraction peaks of α-MnO_2 are slightly lower and broader than that of $CaMnO_3$ because of the relative lower temperature synthesis. The reason that we chose α-MnO_2 nanorods as a reference is that nanostructured α-MnO_2 nanotubes and nanowires have been early reported as the efficient OECs [5, 6]. For $CaMnO_3$, each Mn atom is coordinated by six oxygen atoms with forming MnO_6 octahedra structure. In contrast, all the MnO_6 octahedra are transformed into MnO_5 square pyramids in $Ca_2Mn_2O_5$ due to the loss of oxygen atoms. However, the framework of the perovskite structure is maintained for the $Ca_2Mn_2O_5$. The microstructures of the manganese oxides observed by SEM were shown in Fig. S1. The calcium manganese oxide samples are porous, with an average primary particle size about 50–300 nm. The α-MnO_2 nanorods displayed uniform morphologies with diameters of approximately 50 nm and length of 300 nm. Furthermore, the BET surface areas of $CaMnO_3$, $Ca_2Mn_2O_5$ and MnO_2 were determined to be about 5.19 m^2/g, 5.67 m^2/g and 22.67 m^2/g, respectively.

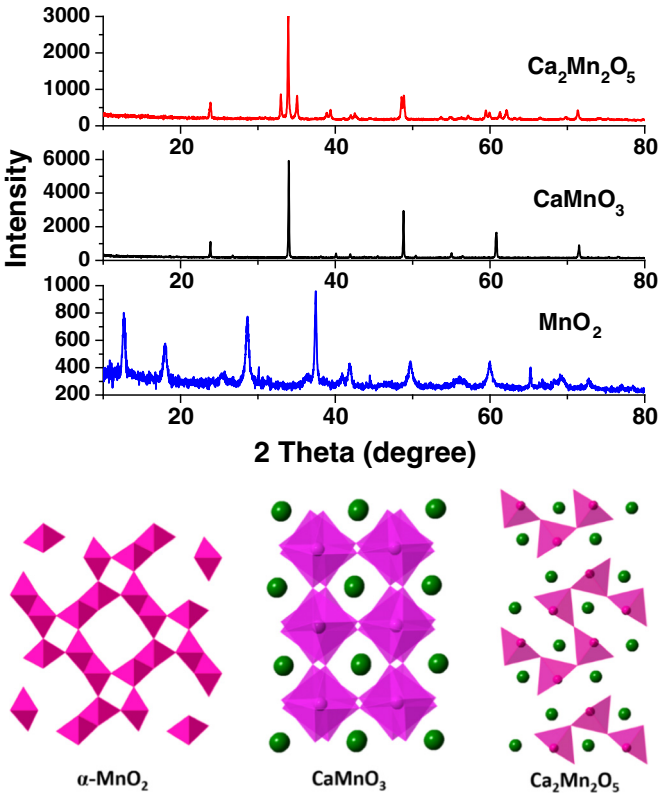

Fig. 1. XRD patterns and illustration of crystal structures of α-MnO_2, $CaMnO_3$ and $Ca_2Mn_2O_5$ (green spheres indicate calcium cations). (For interpretation of the references to color in this figure legend, the reader is referred to the web version of this article.)

3.2. Water oxidation tests

A well-established $Ru(bpy)_3^{2+}$–$S_2O_8^{2-}$ sacrificial water oxidation system was employed to evaluate the photocatalytic performance of manganese oxides [16]. Firstly, experimental conditions for oxygen generation were optimized with varying the concentration of electron acceptor ($Na_2S_2O_8$) and dye sensitizer ($Ru(bpy)_3Cl_2$) with α-MnO_2 as a model catalyst. As shown in Fig. 2a, the concentration of $S_2O_8^{2-}$ varied from 1.0 mM to 50 mM. The highest O_2 yield was obtained with 10 mM $S_2O_8^{2-}$ as the electron acceptor. Further increase of the concentration of $S_2O_8^{2-}$ reduced the O_2 yield, probably because the generation of $[Ru(bpy)_3]^{3+}$ oxidant was too fast to efficiently oxidize water on α-MnO_2 catalyst, as the water oxidation reaction catalyzed by α-MnO_2 is the rate-limiting step in the overall process. Alternatively, the strong oxidants would oxidize the organic ligand to decompose the Ru-dye as a competitive reaction [16]. Fig. 2b depicts the effect of concentration of $Ru(bpy)_3^{2+}$ on the evolution of oxygen. The O_2 yield markedly increased with increasing the concentration from 25 μM to 100 μM. However, further increasing the concentration of $Ru(bpy)_3^{2+}$ to 200 μM slightly enhanced the O_2 yield. Therefore, the conditions of employing 10 mM $S_2O_8^{2-}$ and 100 μM $Ru(bpy)_3^{2+}$ dye were screened out for performing the water oxidation. Under the optimized conditions, different manganese oxide samples were tested for the O_2 evolution as shown in Fig. 2c. The O_2 yields normalized by Mn atoms on the basis of same quantity of catalyst mass indicated that $Ca_2Mn_2O_5$ is the most active catalyst, whereas $CaMnO_3$ and MnO_2 samples exhibited similar performance. In addition, the activities of heterogeneous catalysts are strongly affected by surface areas of solid catalysts [17]. Thus, in most cases, the water oxidation activities among different samples are compared after normalization by the surface area. As shown in Fig. 2d, the normalized O_2

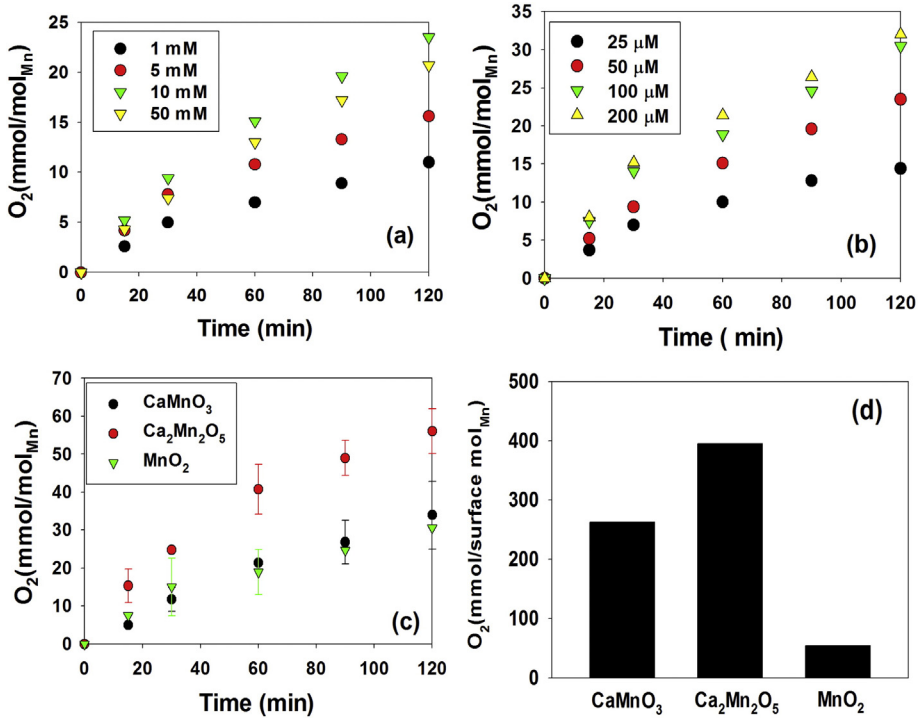

Fig. 2. Visible light photochemical oxygen production with (a) varied concentrations of $Na_2S_2O_8$ using 50 μM Ru dye sensitizer; (b) varied concentrations of Ru dye sensitizers with 10 mM $Na_2S_2O_8$; (c) oxygen production from different catalyst samples with 10 mM $Na_2S_2O_8$ and 100 μM Ru dye sensitizer; (d) Normalized oxygen evolution activity by surface area. All the experiments were performed with 25 mg catalyst in 100 ml pH = 9.0 aqueous buffer solution.

evolution efficiency of the three samples is followed with the order of $Ca_2Mn_2O_5$ > $CaMnO_3$ > α-MnO_2. As shown in Table 1, the TOFs of $Ca_2Mn_2O_5$ sample is 2–3 times higher than those of the $CaMnO_3$ and MnO_2 nanorods, and the TOFs of $Ca_2Mn_2O_5$ normalized by surface area is about one order of magnitude higher than that of MnO_2 nanorods, which confirms that $Ca_2Mn_2O_5$ is the most active catalyst for water oxidation.

The cyclic voltammetry (CV) measurements of manganese oxide samples in 0.1 M aqueous NaOH solution were shown in Fig. S2. A thin TiO_2 layer was used as a supporting layer for deposition of different Mn catalysts. The sharp increase of anodic currents at 0.6 V–0.9 V (vs. Ag/AgCl) can be assigned to water oxidation reaction. The onset potentials for water oxidation are ca. 0.70 V, 0.72 V and 0.72 V for $Ca_2Mn_2O_5$, $CaMnO_3$ and MnO_2, respectively. Compared to the onset potential of bare TiO_2 electrode for the water oxidation (~0.80 V), all the manganese oxide samples exhibited lower onset potentials, confirming that all the manganese oxide samples work as water oxidation catalysts. Oxygen-vacant $Ca_2Mn_2O_5$ exhibits reduced onset potential and increased anodic current compared to $CaMnO_3$ and MnO_2. Furthermore, the O_2 evolution experiments were repeated up to 3 cycles (2 h for each cycle) with the same batch of the catalyst for evaluating the stability of catalysts. As shown in Fig. S3, the O_2 yields were dramatically reduced over 50% and 70% for the $CaMnO_3$ and $Ca_2Mn_2O_5$ samples respectively, whereas the α-MnO_2 exhibited the relatively stable performance during the 3 cycles' tests.

Table 1
Apparent turnover frequency (TOF) of manganese oxide catalysts and selected structural parameters.

Catalyst	BET (m^2/g)	TOF[a] (s^{-1})	TOF[b] (surface) (s^{-1} m^{-2})	Avg. Mn—O distance (Å)
$CaMnO_3$	5.19	0.56×10^{-5}	4.3×10^{-5}	1.900
$Ca_2Mn_2O_5$	5.67	1.70×10^{-5}	1.2×10^{-4}	1.912
α-MnO_2 nanorods	22.7	0.83×10^{-5}	1.5×10^{-5}	1.892

[a] Oxygen evolution rate normalized by manganese atom during the first 15 min reaction after photoirradiation (>420 nm) of an aqueous buffer solution (pH 9, 100 ml) containing 25 mg catalyst, 10 mM $Na_2S_2O_8$ and 100 μM $Ru(bpy)_3Cl_2$.
[b] TOF normalized by manganese atom with same surface area.

3.3. Mechanism analysis

To explore the reasons that are responsible for the enhanced water oxidation activity of $Ca_2Mn_2O_5$ and the rapid deactivation of calcium manganese oxides during the repeated tests. A further investigation on the chemical states and composition of surface Mn, Ca and O of different catalysts before and after reaction was performed by XPS analysis. The Mn *2p* peaks of all the samples are similar (Fig. S4), which can be deconvoluted into a mixture of Mn^{3+} and Mn^{4+}. There was no significant difference for the samples before and after reaction. It is unexpected that the surface Mn in $CaMnO_3$ contains a large portion of Mn^{3+}. The surface composition might be slightly different from the bulk composition. The Ca/Mn atomic ratio is approximately 0.6 according to the XPS analysis (Table S1), implying that the surface of $CaMnO_3$ is composed by a mixture of MnO_x and $CaMnO_3$. Thus, a large fraction of Mn^{3+} would be present on the surface of $CaMnO_3$. On the other hand, the Ca/Mn atomic ratio on the surface of $Ca_2Mn_2O_5$ is approximately 1 (Table S1), in consistent with the theoretical molecular composition. The high temperature reduction process relocated the distribution of Ca and Mn atoms. The presence of Mn^{3+} on α-MnO_2 sample is owing to the occupation of K^+ ions into the α-MnO_2 nanorods during the synthesis, which has been well reported before [6]. Since the oxidation states of Mn are not clearly distinguished among the tested samples, the role of Mn oxidation states in water oxidation could not be inferred. In addition, the contents of calcium ions were significantly reduced even at pH = 9 buffered condition for the $CaMnO_3$ (~50%) and $Ca_2Mn_2O_5$ (100%) after reaction, respectively (Fig. S5 and Table S1). The dissolution of calcium cations was also observed for $CaMn_2O_4 \cdot nH_2O$ during water oxidation process [11]. Due to the dissociation of calcium cations, the surface structure of $CaMnO_3$ and $Ca_2Mn_2O_5$ samples would be dominated by MnO_x or Na_xMnO_y due to the replacement of calcium ions by

sodium ions in buffer, which results in the change of water oxidation efficiency.

Furthermore, the deconvoluted O *1s* spectra of different samples before and after reaction shown in Fig. S6 and Table S1 are quite different. The O *1s* binding energies of the OH^- and O^{2-} components correspond to 531.1 eV and 528.8 eV, respectively. Among these samples, the intensity of hydroxyl peaks follows the order of $Ca_2Mn_2O_5$ > $CaMnO_3$ > MnO_2. After reaction, the intensity of hydroxyl peaks was markedly reduced for $CaMnO_3$ and $Ca_2Mn_2O_5$ samples. The dissolution of calcium ions during the repeated tests could lead to the change of surface hydroxyl group on $CaMnO_3$ and $Ca_2Mn_2O_5$. Thus, we propose that the water oxidation activities of different samples are strongly correlated with the concentration of surface adsorbed hydroxyl groups, according to the water oxidation and XPS analysis results. The increased fraction of surface hydroxyl groups in $Ca_2Mn_2O_5$ enhanced the water oxidation efficiency. The significantly reduced water oxidation activity for $CaMnO_3$ and $Ca_2Mn_2O_5$ could be assigned to the reduction of surface adsorbed hydroxyl groups.

The process of O_2 evolution from water oxidation on a metal centered catalyst can be expressed as shown in [Eqs (1)-(4)]. The formation of O—O bond in —OOH adsorbate on metal ions (step 3) and the deprotonation of the oxyhydroxide group to form peroxide ions (step 4) are regarded as the rate-limiting steps [18].

$$M^{n+} + H_2O\text{---}M^{(n+1)+}\text{—}OH + H^+ + e^- \quad (1)$$

$$M^{(n+1)+}\text{—}OH\text{---}M^{(n+1)+}\text{—}O^{2-} + H^+ + e^- \quad (2)$$

$$M^{(n+1)+}\text{—}O^{2-} + H_2O\text{---}M^{n+}\text{—}OOH^- + H^+ + e\text{—} \quad (3)$$

$$M^{n+}\text{—}OOH^-\text{---}M^{(n+1)+}\text{—}O_2{}^{2-} + H^+ + e^- \quad (4)$$

Accordingly, the O_2 evolution process on a manganese center from $Ca_2Mn_2O_5$ was proposed as shown in Scheme 1. Removing lattice oxygen atoms from $CaMnO_3$ perovskites leads to the change of coordination structure from octahedral to tetrahedral as shown in Fig. 1. The average distance of Mn—O bonds in $Ca_2Mn_2O_5$ is much longer than those in $CaMnO_3$ and α-MnO_2 due to the Jahn-Teller distortion (Table 1). An increased structural distortion arising from oxygen vacancies in $Ca_2Mn_2O_5$ would be beneficial for adsorption of OH^- ions onto the oxygen vacant site on MnO_5 subunit, which results in formation of MnO_5—OH— octahedral unit (step 1) as demonstrated by XPS analysis [18]. The overlapping of e_g orbital of Mn^{3+} and the O-p_σ orbital of OH— also improves the formation of O—O bond and the deprotonation of the oxyhydroxide group (step 3 and 4) [18]. These key structural characteristics of $Ca_2Mn_2O_5$ reduced its onset potential on electrochemical water oxidation and improved its O_2 evolution efficiency compared to $CaMnO_3$ and α-MnO_2.

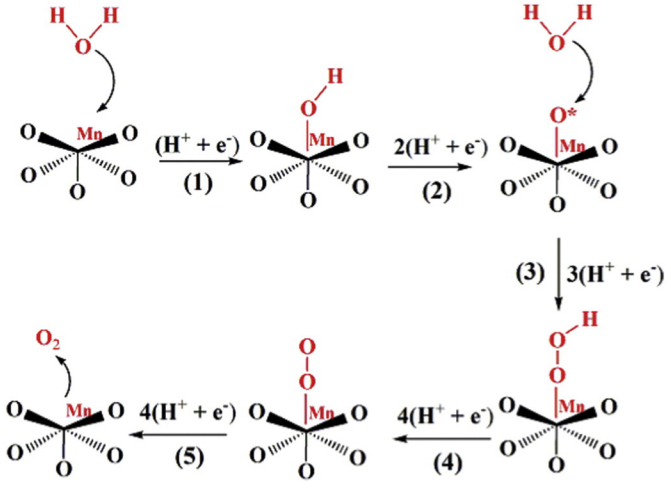

Scheme 1. Illustration of the proposed water oxidation process on a MnO_5 sub-unit in $Ca_2Mn_2O_5$.

4. Conclusions

In summary, $Ca_2Mn_2O_5$ as a biomimetic water oxidation catalyst was evaluated in both photochemical and electrochemical systems. The increased structural distortion arising from oxygen vacancies in $Ca_2Mn_2O_5$ would be beneficial for adsorption of OH^- ions onto the oxygen vacant site on MnO_5 subunit, which was proposed as the main reason to improve its water oxidation performance in comparison with $CaMnO_3$ and MnO_2. Further structural modification of the calcium manganese oxides is suggested to improve their stabilities.

Acknowledgements

We thank the research project of Drinking Water Disinfection Process and Byproducts Control Technology for the support funding (2015ZX07406-004).

Appendix A. Supplementary data

Supplementary data to this article can be found online at http://dx.doi:10.1016/j.catcom.2016.10.035.

References

[1] M.G. Walter, E.L. Warren, J.R. Mckone, S.W. Boettcher, Q. Mi, E.A. Santori, N.S. Lewis, Chem. Rev. 110 (2010) 6446–6473.
[2] M. Yagi, M. Kaneko, Chem. Rev. 101 (2001) 21–35.
[3] M. Suga, F. Akita, K. Hirata, G. Ueno, H. Murakami, Y. Nakajima, T. Shimizu, K. Yamashita, M. Yamamoto, H. Ago, JR. Shen, Nature 517 (2015) 99–103.
[4] E.A. Karlsson, B.-L. Lee, T. Akermark, E.V. Johnston, M.D. Karkas, J. Sun, O. Hansson, J.-E. Backvall, B. Akermark, Angew. Chem. 123 (2011) 11919–11922.
[5] V.B.R. Boppana, F. Jiao, Chem. Commun. 47 (2011) 8973–8975.
[6] V.B.R. Boppana, S. Yusuf, G.S. Hutchings, F. Jiao, Adv. Funct. Mater. 23 (2013) 878–884.
[7] C.-H. Kuo, W. Li, L. Pahalagedara, A.M. El-Sawy, D. Kriz, N. Genz, C. Guild, T. Ressler, S.L. Suib, J. He, Angew. Chem. Int. Ed. 54 (2015) 2345–2350.
[8] K. Jin, J. Park, J. Lee, K.D. Yang, G.K. Pradhan, U. Sim, D. Jeong, H.L. Jang, S. Park, D. Kim, N.-E. Sung, S.H. Kim, S. Han, K.T. Nam, J. Am, Chem. Soc. 136 (2014) 7435–7443.
[9] P.W. Menezes, A. Indra, P. Littlewood, M. Schwarze, C. Gobel, R. Schomacker, M. Driess, ChemSusChem 7 (2014) 2202–2211.
[10] D.M. Robinson, Y.B. Go, M. Mui, G. Gardner, Z. Zhang, D. Mastogiovanni, E. Garfunkel, J. Li, M. Greenblatt, G. Charles Dismukes, J. Am. Chem. Soc. 135 (2013) 3494–3501.
[11] M.M. Najafpour, T. Ehrenberg, M. Wiechen, P. Kurz, Angew. Chem. Int. Ed. 49 (2010) 2233–2237.
[12] F. Rong, J. Zhao, Z. Chen, Y. Xu, Y. Zhao, Q. Yang, C. Li, J. Mater. Chem. A 4 (2016) 6585–6594.
[13] J. Du, T. Zhang, F. Cheng, W. Chu, Z. Wu, J. Chen, Inorg. Chem. 53 (2014) 9106–9114.
[14] J. Kim, X. Yin, K.-C. Tsao, S. Fang, H. Yang, J. Am. Chem. Soc. 136 (2014) 14646–14649.
[15] P. Ragupathy, D.H. Park, G. Campet, H.N. Vasan, S.-J. Hwang, J.-H. Choy, N. Munichandraiah, J. Phys. Chem. C 113 (2009) 6303–6309.
[16] Y. Yamada, K. Yano, D. Hong, S. Fukuzumi, Phys. Chem. Chem. Phys. 14 (2012) 5753–5760.
[17] G.A. Somorjai, Surf. Sci. 299–300 (1994) 849–866.
[18] J. Suntivich, K.J. May, H.A. Gasteiger, J.B. Goodenough, Y. Shao-Horn, Science 334 (2011) 1383–1385.